https://doi.org/10.46813/2026-161-178

STRUCTURAL AND DENSITY CHANGES OF AMORPHOUS FILMS OF ALUMINA AT ELECTRON-BEAM ANNEALING

A.G. Bagmut
National Technical University "Kharkiv Polytechnic Institute",
Kharkiv, Ukraine
E-mail: agbagmut@gmail.com

Amorphous films of alumina (Al_2O_3) were investigated at electron-beam annealing. TEM studies with "in situ" video recording of structural changes demonstrated, that phase transformation of alumina is the island polymorphous crystallization mode with the relative length $\delta_0 \approx 70$. The dependence on time of the fraction of the crystalline phase has an exponential character, described by the JMAK formula with a rate constant $k = 0.058$ s^{-2} and Avrami exponent $n = 2.01$. The density of the crystalline film exceeds the density of the amorphous film. The relative change of the density of the film substance after crystallization is (10.4 ±1.7)%.

PACS: 61.14.−x, 61.43.Dq, 61.72.Cc, 64.70.Kb, 68.37.Lp, 68.55.A−, 68.37.−d

INTRODUCTION

Interest to thin films of alumina (aluminum oxide Al_2O_3) is due to their use in microelectronics, protective coatings, and catalysis [1]. They have high values of permittivity, good adhesion and time stability of parameters [2]. At present, special attention is paid to the study of amorphous films of Al_2O_3. They are the key material in optical coatings due to its broad transparency window (ultraviolet to mid-infrared) and excellent durability [3]. Various physical and chemical deposition methods are used to obtain amorphous films of Al_2O_3. These include sol-gel, chemical vapor deposition (CVD), pulsed laser deposition (PLD), atomic layer deposition (ALD), e-beam evaporation and plasma-assisted reactive magnetron sputtering (PARMS) [3–6].

To manufacture products with optimal parameters, a necessary condition is knowledge of the patterns of their change from influencing factors, for example, from the ambient temperature. Subsequent annealing, which is required at the industrial production stage or natural aging can initiate undesirable crystallization of the amorphous layer. The crystallization of coatings results in a rough microstructure and surface, which significantly affects the optical and electrical properties [7].

Research indicates that both the annealing temperature and duration are pivotal in the crystallization process. A critical temperature exists, above which amorphous Al_2O_3 transitions to its crystalline form. For instance, studies have shown that annealing amorphous Al_2O_3 films at temperatures exceeding 800°C leads to crystallization into γ-Al_2O_3 and other phases such as δ-Al_2O_3. The transformation from amorphous to crystalline (a-c transformation) Al_2O_3 typically follows a sequence of phase changes. The proposed temperature-dependent sequence is: amorphous → γ → δ → θ → α-Al_2O_3. However, other pathways may occur depending on the starting material and specific conditions. For instance, X-ray diffraction studies have shown that annealing in nitrogen can crystallize ALD-deposited Al_2O_3 films into the monoclinic θ-Al_2O_3 at 800 and 1000 °C [1, 2, 8]. Heat treatment of amorphous films and coatings is accompanied not only by structural, but also by volumetric changes, leading to a disruption of the continuity and homogeneity of the protective layer [2]. Therefore, the study of volume changes and crystallization kinetics of amorphous films of alumina would provide beneficial knowledge required for complete control of the deposition process.

The aim of this work was to study the structural and volumetric changes, as well as the kinetics of crystallization during electron beam annealing of amorphous alumina films. Determination of kinetic parameters of crystallization will make it possible to numerically classify the type of a-c transformation. TEM study with in situ video registration of structural evolution offers the possibility do it.

EXPERIMENTAL SECTION

The samples were free-standing amorphous films of alumina. They were obtained by pulsed laser sputtering of rotary Al target in an oxygen atmosphere ($P(O_2)$ ~ 0.13 Pa) and by subsequent deposition of vapor-plasma flow on the substrate of (001) KCl at room temperature. The target was sputtered by pulses of radiation of ÀIG: Nd^{3+} laser (LTIPCH-5), operating in a Q-switched mode. The laser wavelength and the pulse repetition rate were 1.06 μm and 25 Hz correspondingly. The oxygen in the evaporation chamber was embedded using a specialized system for gas introduction SNA-2 of JSC "SELMI" (Sumy, Ukraine). The film thickness was defined based on the number of impulses of laser irradiation influencing the sprayed target. It was transparent to the electron beam and had a thickness ≈ 25 nm. The obtained films were separated from the substrates in distilled water and placed on the micro grids for the following electron diffraction and electron microscopic investigations.

Features of the a-c phase transformation were studied by selected area electron diffraction (SAED) and transmission electron microscopy (TEM) at the accelerating voltage of 100 kV.

Crystallization of alumina was initiated with electron beam annealing of the film on a subject microgrid (grid mesh 270) inside the microscope column (Fig. 1,a). This made it possible to register the

structural transformations in situ. Besides using an electron beam focused to a diameter of 2…5 mm at beam current of 20 mA, one can perform the beam density j varying from 6.37 A/mm^2 (dose rate ~ $39.8 \cdot 10^4$ e$^-$/(Å^2·s)) to 1.02 A/mm^2 (dose rate ~ $6.4 \cdot 10^4$ e$^-$/(Å^2·s)) for different heating conditions. The crystallization process was recorded with a Canon Power Shot G15 camera at the frame rate of 30 s^{-1} (Fig. 1,b).

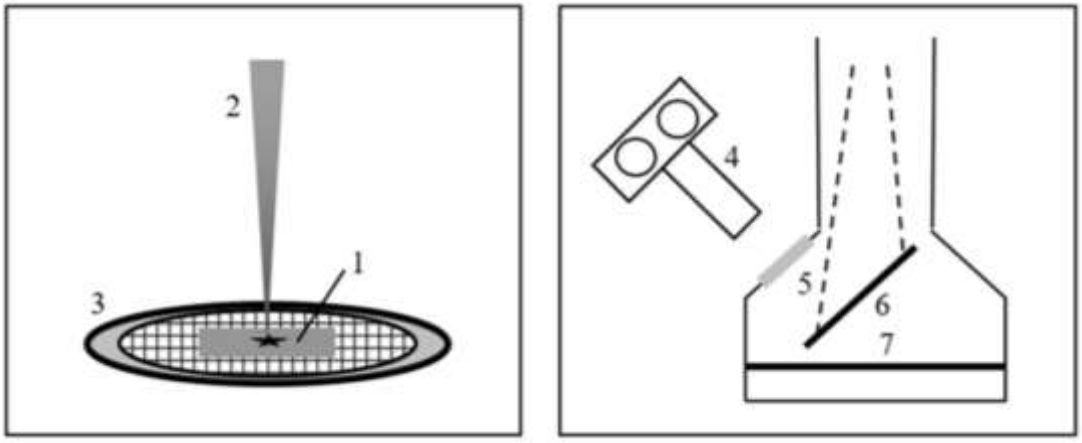

a *b*

Fig. 1. Scheme of the electron-beam crystallization (a) and video recording of the crystallization process (b): 1 – amorphous film; 2 – electron beam; 3 – object grid; 4 – video camera; 5 – viewing window; 6 – photoluminescent screen; 7 – photographic plate

According to [9] using a specialized computer program, we measured the total area, occupied by the crystals at the electron microscope image of the analyzed space of the film. The content of the crystalline fraction x in the video frame we defined as the ratio

$$x = \frac{S(t)}{S_f}, \quad (1)$$

where $S(t)$ is the area occupied by the crystalline phase in the frame at an arbitrary time moment t and S_f is the area of the field of the study. The crystal diameter $D(t)$ at a time t was determined according to the relation

$$D(t) = \sqrt{\frac{4S_k(t)}{\pi}}, \quad (2)$$

where $S_k(t)$ is the area of the crystal image at the time t. The average size of the crystals:

$$\langle D \rangle = \frac{1}{N}\sum_1^N D_i, \quad (3)$$

where D_i is the diameter of a single crystal, taken at number of i.

The structural state of amorphous medium is characterized with the presence of unconfined space – part of the whole volume of the solid, which is not completed with the particles of matter. In kinetic aspect unconfined space represents the part of volume, allowing the motion of the particles of material. So, the occurrence of the unconfined space may be experimentally revealed at annealing of amorphous film as the change of the relative density η, determining as:

$$\eta = \frac{\rho_c - \rho_a}{\rho_a}. \quad (4)$$

In expression (4) ρ_a is the substance density before transformation (amorphous); ρ_c is the substance density after transformation (crystalline). In amorphous state the value of the unconfined space as a rule exceeds the value of the unconfined space in crystalline one, because the crystalline state can be characterized with ordered disposition of atoms (molecules). As a rule,

$$\eta > 0.$$

Laser sputtering provided the formation of micro-drops of sputtered substance in condensed film. This micro-drop we used as bench marks. The distance L_a between them in amorphous state was changed, and after crystallization it was L_c. So, performing the measurements of L_a and L_c, the η according to (4) can be calculated as [10]:

$$\eta = \left(\frac{L_a}{L_c}\right)^3 - 1. \quad (5)$$

RESULTS AND DISCUSSION

A TEM image of a partially crystallized film of alumina is shown at Fig. 2. After separation from the substrate of KCl the film was amorphous. This is evidenced by the SAED picture in the lower right corner of the image. It consists of two diffraction halos. The first halo is intense, while the second halo is much weaker in the intensity and very diffuse. The action of the electron beam initiates in it growth ofdisoriented crystals, as evidenced by the SAED pattern in the upper right corner of the image.

According to it the crystalline phase of alumina corresponds to the cubic modification γ-Al_2O_3 with the unit cell parameter a_0 = 0.7924 nm [11]. Crystallization of the amorphous alumina is accompanied by increasing of the density of the film material.

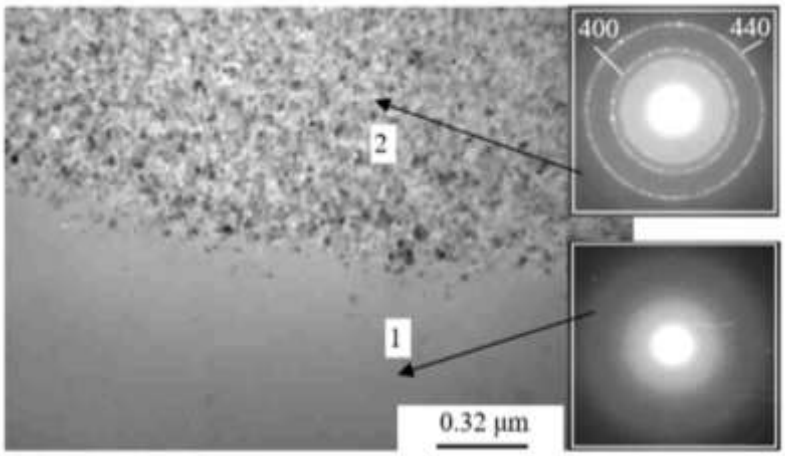

Fig. 2. Electron-beam crystallization of the amorphous Al_2O_3 film: TEM image of the film after partial crystallization; SAED of the amorphous part of the film (in the lower right corner of the image) and SAED patterns of the crystallized part of the film (in the upper right corner of the image.): 1 – amorphous phase, 2 – crystalline phase

Fig. 3 shows two micrographs of the same section of the Al_2O_3 film in the initial amorphous state (a) and after its complete crystallization by an electron beam (b). The film contains microdroplets of Al, brought from the target to the substrate by the vapor-plasma flow. This is a manifestation of the so-called "splash effect", characteristic of the laser deposition method. They are rigidly connected to the film and are marked with numbers from 1 to 4. The length of the lines connecting the aluminum microdroplets in amorphous (see ${}^{ik}L_a$ at Fig. 3,a) and crystalline (see ${}^{ik}L_c$ at Fig. 3,b) film is different. As a rule ${}^{ik}L_a > {}^{ik}L_c$. At Fig. 3 indices i and k ($i \neq k$) take values from 1 to 4. The value of η can be determined by substituting the numerical values of distances between adjacent marks of ${}^{ik}L_a$ and ${}^{ik}L_c$ into (5).

If there are n marks on each of the micrographs, then the number of possible measurements of the distances between the marks before and after crystallization (i.e. ${}^{ik}L_a$ and ${}^{ik}L_c$) will be $\frac{n(n-1)}{2}$. In this case, according to (5), we obtain $\frac{n(n-1)}{2}$ different values of η. In our case for n=4 possible measurements equal to 6. According to (5) each pair of distances ${}^{ik}L_a$ and ${}^{ik}L_c$ corresponded to one value of ${}^{ik}\eta$. The following data were obtained: ${}^{12}\eta$ = 8.6%, ${}^{13}\eta$ = 7.5%, ${}^{32}\eta$ = 15.3%, ${}^{42}\eta$ = 11.7%, ${}^{43}\eta$ = 13.0%, ${}^{14}\eta$ = 6.4%. Arithmetic mean <η>= 10.4%. For 6 measurement relative change of the density of alumina η = (10.4 ±1.7)%. That is, with a probability of 70%, the true value of η is in the range from 8.7% to 12.1%. According to [2], at 600 °C amorphous alumina has a density ρ_a = 3.25 g/cm^3. After crystallization at 800°C its density increases and is ρ_c = 3.55 g/cm^3. In this case, according to (4) η = 9.2%, that fits well into our range from 8.7 to 12.1%.

Based on the frame-by-frame analysis of the video, the dependence on time t of the number density of crystals N was obtained. At a fixed electron dose rate N increases linearly with time. The dependence $N(t)$ is shown at Fig. 4,a. Straight line correspond to the equation:

$$N = 5.13\cdot10^9 t + 2.50\cdot10^9 \text{ cm}^{-2}, \quad (6)$$

where t is measured in seconds. According to (6) the nucleation rate $\alpha = 5.13\cdot10^9$ cm$^{-2}\cdot$s^{-1}.

The dependences on time of the average crystal diameter <D> is shown at Fig. 4,b. Straight line correspond to the equations:

$$<D> = 0.013t + 0.026 \text{ μm}. \quad (7)$$

According to (7) the average crystal growth rate <v> = 0.013 μm·s^{-1}. Data relating to α and <v> are given in Table.

Time dependence of the crystallized volume fraction $x(t)$ is shown at Fig. 5,a. This experimental data, presented in the coordinates ln[-ln(1-x)] – ln$t$, form a straight line (Fig. 5,b). This fact indicates the applicability to the process of a-c phase transformation of the classic Johnson-Mehl-Avrami-Kolmogorov (JMAK) theory through the equation:

$$x(t) = 1\text{-}\exp(-kt^n), \quad (8)$$

where k is a rate constant and n is the Avrami exponent, which is sensitive to the time-dependence of nucleation and to the dimensionality of growth [12–14]. Drawing ln[-ln(1-x)] against ln(t) should be straight line:

$$\ln[-\ln(1-x)] = n\ln t + \ln k. \quad (9)$$

In this case n is the tangent of the angle of inclination of the line to the abscissa and the point of the intersection with the ordinate is ln$k$. The graph at Fig. 5,b corresponds to the equation:

$$\ln[-\ln(1-x)] = 2.01\ln t - 2.85. \quad (10)$$

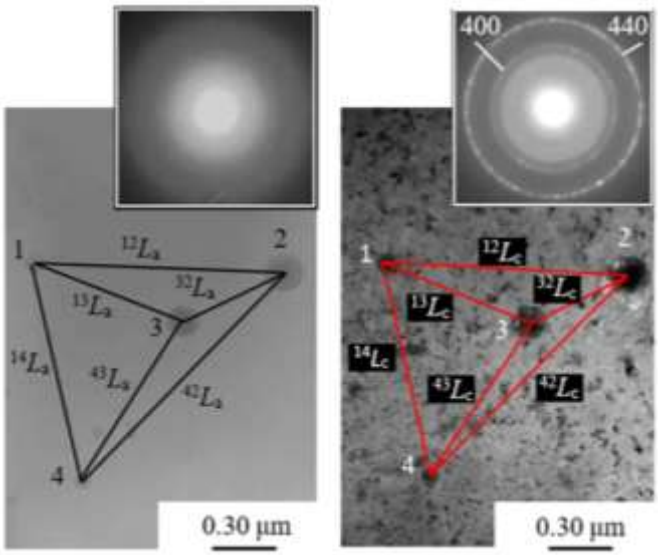

a *b*

Fig. 3. Phase transition from amorphous (a) to crystalline (b) structure in Al_2O_3 film after electron beam crystallization in situ. The lines connect the positions of conjugated microdroplets of Al in the amorphous and crystalline films. SAED pictures are shown in the upper right corner of each micrograph

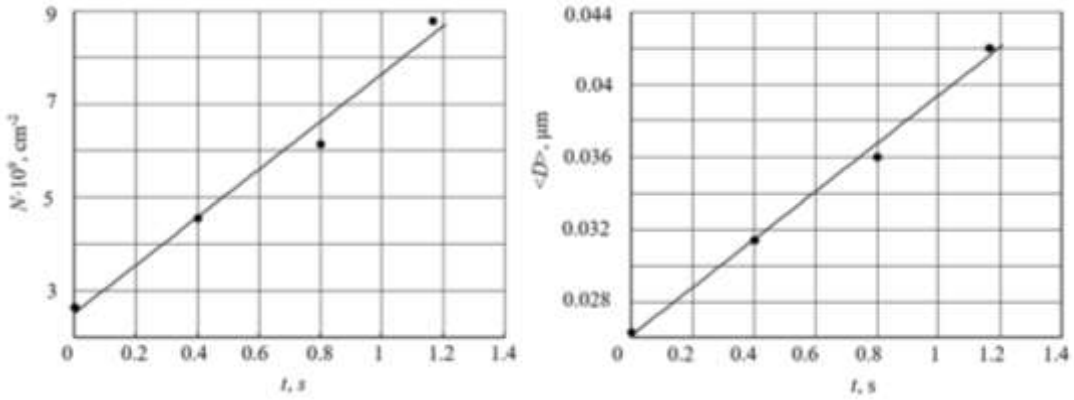

a *b*

Fig. 4. The dependence on time of the number density of crystals N (a) and of the average diameter <D> (b) at crystallization of amorphous Al_2O_3 film

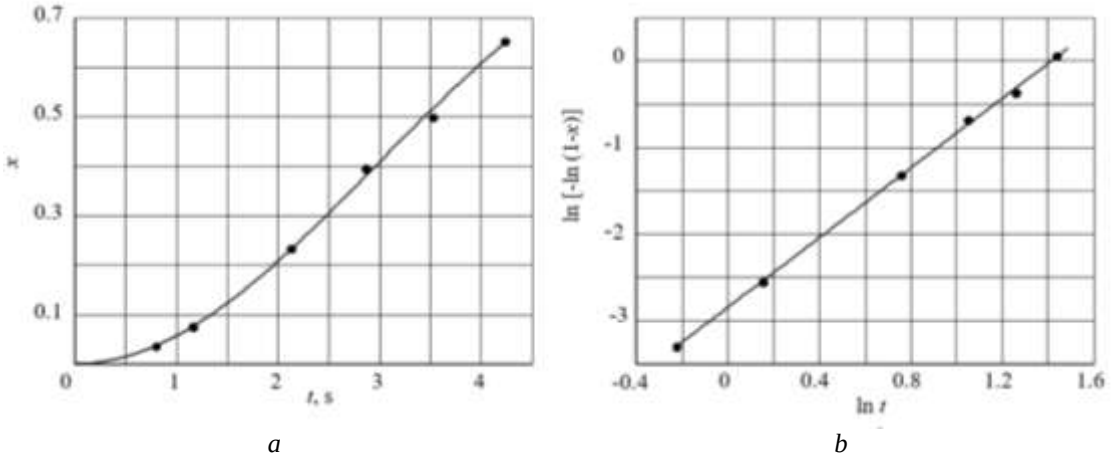

a *b*

Fig. 5. The dependence on time of the crystallized volume fraction x(t) of amorphous Al_2O_3 film in coordinates x – t (a) and in coordinates ln[-ln(1-x)] – lnt (b)

According to (10) and Fig. 5,b n = 2.01, ln$k$ = -2.85 and k = 0.058 s^{-2}. Taking into account numerical values of n and k, the curve at Fig. 5,a will fit the equation:

$$x = 1\text{-}\exp(-0.058t^{2.01}). \quad (11)$$

Data relating to n and k are given in Table.

Parameters of the electron beam induced crystallization of amorphous films of Al_2O_3*

<v>, μm/s	0.013
t_0, s	4.12
D_0, μm	0.054
n	2.01
K, s^{-2}	0.058
α, $cm^{-2}\cdot s^{-1}$	$5.13\cdot10^{9}$
δ_0	70

*<v> is the average tangential growth rate of the crystals; t_0 is the characteristic time unit; D_0 is the characteristic length unit; n is the Avrami exponent, k is the rate constant; α is the nucleation rate; δ_0 is the relative length.

CONCLUSIONS

Amorphous films of alumina are formed on substrates at room temperature in the process of pulsed laser sputtering of Al targets in an oxygen atmosphere. Irradiation of amorphous film with the electron beam initiates its crystallization. The transformation has one-stage character. The amorphous alumina polymorphically passes into the crystalline one with cubic modification γ-Al_2O_3. According to TEM and SAED data (see Fig. 2) during crystallization of the film multiple crystals grows in the field of observation and a polycrystalline film is formed. The density of the crystalline film exceeds the density of the amorphous film. The relative change of the density of the film substance after crystallization is (10.4 ±1.7)%.

The case α = const and <v> = const corresponds to the α-version of Kolmogorov's model [15]. This is the case of the continuous nucleation, when the system keeps adding nuclei with the same rate over the entire transformation period [16]. The dependence of the fraction of the crystalline phase x on time t has an exponential character, described by the JMAK formula. The Avrami exponent n = 2.01 (nearest integer is 2). However, these values of n = 2 is typical for the crystallization process in which grain growth occurs without nucleation and crystallization is called "site saturation". All the nuclei present in the amorphous medium begin to grow at the beginning of the a-c transformation [16]. This situation was realized in experiments on electron-beam crystallization of amorphous ZrO_2 films deposited by laser evaporation [17].

The value of the Avrami exponent in this study should be n = M+1 = 3 because the nucleation rate is constant and growth dimensionality in thin film state M = 2 [12]. This discrepancy can be explained by a decrease of the nucleation rate with progress of the grain growth due to the action of tensile stresses [18]. The occurrence of tensile stresses in the crystallizing alumina film is due to an increase in its density (η = 10.4%), that is experimentally confirmed in this work.

In the case of a polymorphous transformation, each crystallization mode can be quantitatively characterized by a numerical criterion – the dimensionless relative length of crystallization δ_0 [19]. The relative length of crystallization defined as

$$\delta_0 = \frac{D_0}{\sqrt[3]{\Omega}}. \qquad (12)$$

D_0 is a characteristic unit of length – the conditional size of a crystal by the time t_0, after which the volume of the amorphous phase decreases by a factor of e = 2.718 (the so-called characteristic unit of time). In this case, the fraction of crystallized substance x = 0.632. In expressions (12) Ω is the volume of a unit cell of a crystal, growing in amorphous matrix.

In the case of Al_2O_3 when x = 0.632 according to (11) the characteristic unit of time t_0 = 4.12 s. Characteristic unit of the length D_0= <v> $t_0 \approx$ 0.054 μm. For Al_2O_3 the volume of unit cell Ω = $4.9755\cdot10^{-10}$ μm^3 [11]. In this case, according to (12), the relative length $\delta_0 \approx 70$ (number corresponding to the island polymorphous crystallization mode [20]).

REFERENCES

1. H. Qin, P. Sutter, G. Zhou. The Crystallization of Amorphous Aluminum Oxide Thin Films Grown on NiAl (100) *// J. Am. Ceram. Soc*. 2014, v. 97, p. 2762-2769; https://doi.org/10.1111/jace.13036

2. M. Broas, O. Kanninen, V. Vuorinen, M. Tilli, M. Paulasto-Kröckel. Chemically Stable Atomic-Layer-Deposited Al_2O_3 Films for Processability // *ACS Omega*. 2017, v. 2, p. 3390-3398; https://pubs.acs.org/doi/10.1021/acsomega.7b00443

3. P. Ahmadi, M. Chesaux, J. Wojcik, D. Deligiannis, P. Mascher, J. Bradley. Low-loss and low-temperature Al_2O_3 thin films for integrated photonics and optical coatings *// J. Vac. Sci. Technol A.* 2024, v. 42, p. 063402-1 - 063402-9; https://doi.org/10.1116/6.0003976

4. Y. Lin, C. Cheng, L. Young, L. Chiang, W. Chen, K. Lai, S. Chiu, C. Wu, C. Liang, J. Lin, C. Hsu, Y. Lin, J. Kwo, M. Hong. Nanometer-thick molecular beam epitaxy Al films capped with in situ deposited Al_2O_3–High-crystallinity, morphology, and superconductivity // *J. Appl. Phys.* 2024, v. 136, p. 074401-01-074401-08; https://doi.org/10.1063/5.0213941

5. Y. Lan, Y. Zou, X. Ma1, L. Xu, L. Shi, J. Zhang. Fabrication of amorphous Al_2O_3 optical film with various refractive index and low surface roughnes // *Mater. Res. Express.* 2020, v. 7, p. 086405-1-086405-6; https://doi.org/10.1088/2053-1591/abb0af

6. M.K. Smit, G.A. Acket, C.J. van der Laan. Fabrication of amorphous Al_2O_3 optical film with various refractive index and low surface roughness // *Thin Solid Films*. 1986, v. 138, p. 171-181; https://doi.org/10.1016/0040-6090(86)90391-3

7. L. Zhang, J. Zhang, H. Jiao, G. Bao, Z. Wang, X. Cheng. Thickness-dependent surface morphology and crystallization of HfO_2 coatings prepared with ion-assisted deposition // *Thin Solid Films*. 2017, v. 642, p. 359-363; https://doi.org/10.1016/j.tsf.2017.10.010

8. V. Miikkulainen. M. Leskelä, M. Ritala, R. Puurunen. Crystallinity of Inorganic Films Grown by Atomic Layer Deposition: Overview and General Trends // *J. Appl. Phys.* 2013, v. 113, p. 021301; https://doi.org/10.1063/1.4757907

9. A. Bagmut, I. Bagmut. In situ crystallization of amorphous Sb_2Se_3 films at electron beam irradiation // *Molecular Crystals and Liquid Crystals*, 2024. v. 768, p. 63-71;
https://doi.org/10.1080/15421406.2024.2309774

10. A. Bagmut, V. Zhuchkov, V. Kolosov, V. Kosevich, D. Melnichenko. Characterization of nanocrystals in laser condensates deposited trough vanadium evaporation in an oxygen atmosphere // *Crystallography Reports*. 2006, v. 51, p. S150-S157; https://link.springer.com/article/10.1134/S1063774506070224

11. *Powder Diffraction File* (Joint Committee on Powder Diffraction Standards, International Center for Diffraction Data, Swarthmore, Philadelphia, United States, 1996), Card No. 29-0063.

12. M. Moghadam, P. Voorhees. Thin film phase transformation kinetics: from theory to experiment // *Scripta Materialia*. 2016, v. 124, p. 164-168;
https://doi.org/10.1016/j.scriptamat.2016.07.010

13. G. Ruitenberg, A.K. Petford-Long, R.C. Doole. Determination of the isothermal nucleation and growth parameters for the crystallization of thin $Ge_2Sb_2Te_5$ films // *J. Appl. Phys.* 2002, v. 2, p. 3116-3123; https://doi.org/10.1063/1.1503166

14. N. Ohshima. Crystallization of germanium-antimony-tellurium amorphous thin film sandwiched between various dielectric protective films // *J. Appl. Phys.* 1996, v. 79, p. 8357-8363;
https://doi.org/10.1063/1.362548

15. A.N. Kolmogorov. *Bull. of the Acad. of Sciences of the USSR, Mathematics Series*, 1, 1937, p. 355; https://www.scirp.org/(S(i43dyn45teexjx455qlt3d2q))/reference/ReferencesPapers.aspx?ReferenceID=880675

16. M. Castro, F. Domı´nguez-Adame, A. Sa´nchez, T. Rodrı´guez. Model for crystallization kinetics: Deviations from Kolmogorov–Johnson–Mehl–Avrami kinetics // *Appl. Phys. Lett.* 1999, v. 75, p. 2205-2207; https://doi.org/10.1063/1.124965

17. A.G. Bagmut. Radiation enhanced crystallization of amorphous laser condensates of hafnia and zirconia // *Problems of Atomic Science and Technology*. 2025, N 2(156), p. 43-48; https://doi.org/10.46813/2025-156-043

18. K.-H. Min, R. Sinclair, I.-S. Park, S.-T. Kim, and U.-I. Chung. Crystallization behaviour of ALD-Ta_2O_5 thin films: the application of in-situ TEM // *Phil. Mag.* 2005, v. 85 p. 2049-2063;
https://doi.org/10.1080/14786430500036546

19. A.G. Bagmut. Crystallization of amorphous Sb_2Se_3 films according to TEM with in situ video recording // *Funct. Mater.* 2024, v. 31, N 1, p. 18-25;
https://doi.org/10.15407/fm31.01.18

20. A. Bagmut. Layer, island and dendrite crystallizations of amorphous films as analogs of Frank-van der Merwe, Volmer-Weber and Stranski-Krastanov growth modes // *Func. Mater*. 2019, v. 26, p. 6-15; https://doi.org/10.15407/fm26.01.6

.

Article received 17.09.2025

ЗМІНИ СТРУКТУРИ ТА ГУСТИНИ АМОРФНИХ ПЛІВОК ОКСИДУ АЛЮМІНІЮ У РАЗІ ЕЛЕКТРОННО-ПРОМЕНЕВОГО ВІДПАЛУ

О.Г. Багмут

Досліджено аморфні плівки оксиду алюмінію (Al_2O_3) у разі електронно-променевого відпалу. Дослідження ПЕМ із відеореєстрацією структурних змін «in situ» показали, що кристалізація оксиду алюмінію є острівцевим поліморфним перетворенням із відносною довжиною $\delta_0 \approx 70$. Залежність від часу частки кристалічної фази має експоненціальний характер, який описується формулою JMAK із константою швидкості k = 0,058 c^{-2} і показником Аврамі n = 2,01. Щільність кристалічної плівки перевищує щільність аморфної плівки. Відносна зміна щільності плівкової речовини після кристалізації становить (10,4±1,7)%.